AB

PRE 29792

π^+p and K$^+$p Elastic Scattering at 250 GeV/c

NA22 Collaboration

Aachen[a]- Berlin(Zeuthen)[b]- Brussels/Antwerp[c]- Helsinki[d]- Krakow[e]- Moscow[f]- Nijmegen[g]- Rio de Janeiro[h]- Serpukhov[i]- Warsaw[j]- Yerevan[k]

M.ADAMUS[j], I.V. AJINENKO[i], N.M.AGABABYAN[k], Y.A. BELOKOPYTOV[i], H. BÖTTCHER[b], P.V. CHLIAPNIKOV[i], F. CRIJNS[g], A. DE ROECK[c,1] E.A. DE WOLF[c,2], K. DZIUNIKOWSKA[e], V.G.GAVRJUSEV[f], A.M.F. ENDLER[h], G.V. GEVORKYAN[i,k], H. GRÄSSLER[a], P. van HAL[g], W. KITTEL[g], Z.A.KIRAKOSYAN[k], D.KISIELEWSKA[e], J.KLUGOW[b], A.I. KURNOSENKO[i], F. MEIJERS[g], A.B. MICHALOWSKA[c] V.I. NIKOLAENKO[i], L.C.S. OLIVEIRA[h], K. OLKIEWICZ[e], L.P. PETROVYKH[i], E. RIIPINEN[d], H.E.ROLOFF[b], V.M.RONJIN[i], A.M.RYBIN[i], H.M.T. SAARIKKO[d], Y.T.M. SAARIKKO[d], W. SCHMITZ[a], L. SCHOLTEN[g], N.A. SOTNIKOVA[f], O.G. TCHIKILEV[i], V.A. UVAROV[i], F. VERBEURE[c], R. WISCHNEWSKI[b], A. WRÓBLEWSKI[j]

ABSTRACT. Results are presented on π^+p and K^+p elastic scattering at 250 GeV/c, the highest momentum so far reached for positive meson beams. The experiment (NA22) was performed with the European Hybrid Spectrometer. The π^+p elastic cross section stays constant with energy while the K^+p cross section increases.

In this paper we report on a study of π^+p and K^+p elastic scattering at 250 GeV/c, the highest energy so far reached for positive meson hadron collisions.

The experiment (NA22) has been performed at CERN in the European Hybrid Spectrometer (EHS) with the Rapid Cycling Bubble Chamber (RCBC), filled with H_2, as a vertex detector, and exposed to a 250 GeV/c tagged positive meson enriched beam. The data were taken with a minimum bias interaction trigger. The experimental setup and the trigger conditions are detailed in [1]. Secondary charged particle tracks are reconstructed from hits in the wire- and drift-chambers of the spectrometer and from tracks measured in

[a] III. Physikalisches Institut B, RWTH, D-5100 Aachen, Federal Republic of Germany

[b] Institut für Hochenergiephysik der Akademie der Wissenschaften der DDR, DDR-1615 Berlin-Zeuthen, German Democratic Republic

[c] Inter-University Institute for High Energies, B-1050 Brussels and Dept. of Physics, Universitaire Instelling Antwerpen, B-2610 Wilrijk, Belgium

[d] Department of High Energy Physics, University of Helsinki, SF-00170 Helsinki, Finland

[e] Institute of Physics and Nuclear Techniques of the Academy of Mining and Metallurgy and Institute of Nuclear Physics, PL-30055 Krakow, Poland; partially supported by grants from CPBP 01.06 and 01.09

[f] Moscow State University, SU-117234 Moscow, USSR

[g] University of Nijmegen and NIKHEF-H, NL-6525 ED Nijmegen, The Netherlands

[h] Centro Brasileiro de Pesquisas Fisicas, Rio de Janeiro, Brazil

[i] Institute for High Energy Physics, SU-142284 Serpukhov, USSR

[j] University of Warsaw and Institute of Nuclear Problems, PL-00681 Warsaw, Poland

[k] Institute of Physics, SU-375036 Yerevan, USSR

the bubble chamber. The majority of protons with laboratory momentum $p < 400$ MeV/c stop inside the bubble chamber. Their momentum is determined from the range in the chamber liquid. The overall $< \Delta p/p >$ for fast secondary tracks and recoil protons is $\leq 2\%$ and $\leq 5\%$, respectively.

Elastic events are selected on the basis of 4–constraint (4C) kinematic fits to the two-prong event sample, using the HYDRA kinematics package. The data samples consist of 1947 π^+p and 2157 K^+p events corresponding to 30% and 100% of our total statistics.

The probability distribution (not displayed) shows the usual peak for $P(\chi^2) < 2\%$ due to poor measurements and inefficiencies in the kinematics program. These low probability events are found not to introduce biases and have been retained in the analysis.

To estimate losses of truely elastic events for which no acceptable kinematic fit is obtained, we calculate for each two-prong the missing mass squared MM^2 of the event and the laboratory angle β between the measured momentum of the scattered beam particle and its momentum predicted from the recoil proton momentum, assuming the event to be elastic. In total, 87% of fitted elastic events fall into the kinematic region

$$-0.15 < MM^2 < 0.15\,\mathrm{GeV}^2 \text{ and } -0.5 < \beta < 0.3 \text{ mrad.}$$

Henceforth we assume that unfitted two-prong events without associated V^0's or γ's falling into this kinematic region are elastic events and can be added to the sample of fitted events. This sub-sample contains 122 π^+p and 132 K^+p events.

At high energies, 4C-fit reactions may still be contaminated by reaction channels with one or several π^0's. This bias is studied in the sample of fitted elastic events which nevertheless have associated neutrals: a 3C-fit γ observed in RCBC and pointing to the primary vertex, or a forward π^0 identified in the lead-glass detectors of EHS, fitted to the event vertex and also satisfying the 4C-fit hypothesis meson $+ p \rightarrow$ meson $+ p + \pi^0$. The corresponding contamination is estimated to be $(2.4 \pm 1.6\%)$ and $(2.8 \pm 2.0\%)$ for π^+p and K^+p elastic events, respectively.

The interaction trigger system includes a vertically mounted scintillator strip, 20 mm wide and located at 12.6 m downstream from the center of RCBC, at a horizontal focus of the beam. The trigger vetoes an elastic collision whenever the scattered beam particle hits the scintillator strip. This not only limits our acceptance in invariant momentum transfer squared to $|t| \geq 0.06$ GeV^2, but also introduces a significant loss of events in the interval $0.06 < |t| < .1$ GeV^2. This trigger loss is corrected for, on an event by event basis, by a geometrical weighting procedure based on the isotropy in azimuthal angle of the scattered beam particle with respect to the incident beam.

For the calculation of absolute cross sections, we use the following procedure. The weighted t-distributions dN/dt of the elastic data samples are fitted to the quadratic exponential form $A \exp(Bt + Ct^2)$ in the intervals $0.06 < -t < 0.98$ GeV^2. The lower $-t$ limit is chosen to avoid the losses at small-$|t|$. The absolute scale of the cross section is then obtained by normalizing the distribution dN/dt at $t = 0$ to the value of the Optical Point (O.T.P.) $= \sigma_{\text{tot}}^2/16\pi$, calculated from the Optical Theorem. We herewith neglect the real part of the forward elastic scattering amplitude. Dispersion relation calculations[**2**] indeed show at this energy that $|\rho| < 0.1$ at $t = 0$; ρ represents the ratio of the real to imaginary part of the elastic amplitude.

Figs. 1a,b show the $d\sigma/dt$ distributions obtained for π^+p and K^+p elastic scattering. The solid lines are fits to the quadratic exponential given above. The fit includes the calculated (O.T.P.) as a data point with a 2% error. The fitted values of the parameters A, B and C are collected in Table 1. The slopes of the differential cross section at $t = -0.2$ GeV^2, $B(t = -0.2\text{GeV}^2)$ are compiled in Figs. 2a,b. The "shrinkage" of the diffractive elastic peak, exhibited by the data, is well parametrized by the form $a + b \ln s/s_0$ ($s_0 = 1$ GeV^2), with $a = (6.3 \pm 0.4)$ GeV^{-2}, $b = (0.36 \pm 0.07)$ GeV^{-2} for π^+p, and $a = (5.5 \pm 0.6)$ GeV^{-2}, $b = (0.3 \pm 0.1)$ GeV^{-2} for K^+p elastic scattering.

Using the results of the fits, we calculate the total elastic cross sections by integrating $d\sigma/dt$ in the interval $0 < |t| < B/2C$ GeV^2. The values of σ_{tot}[**1**], σ_{el} and their ratio are given in Table 2. The errors on σ_{el} include estimates of systematic uncertainties.

A compilation of total elastic cross sections for π^+p and K^+p interactions is shown in Figs. 3a,b. The data at lower energies are taken from the "Hepdata/Compas" data-bases described in [**3**]. The π^+p elastic cross section is, within errors, independent of energy in the s-range between 50 and 500 GeV^2. In the same range, the K^+p elastic cross section increases with about the same rate as the K^+p total cross section. Note that the ratios $\sigma_{\text{el}}/\sigma_{\text{tot}}$ are the same for π^+p and K^+p (Table 2).

Acknowledgements. *We are grateful to the EHS coordinator, L. Montanet, for his interest in our experiment. It is a pleasure to thank the operating crews and staffs of EHS, SPS and the H2 beam, as well as the scanning and measuring and data-handling teams of our laboratories for their invaluable help with this experiment.*

REFERENCES

[1] M.Adamus et al.: *Z. Phys. C—P*[illegible]

[2] R.E.Hendrik and B.Lautrup: *Phys. Re*[illegible]

[3] F.D.Gault: *Comp. Phys. Comm.* 33, [illegible] *Comp. Phys. Comm.* 33, 225 (1984)

Table 1. Parameters values from fits of the function [illegible] to the elastic differential cross section $d\sigma/dt$ at 250 GeV/c

Parameters	π^+p	K^+p
A (mb/GeV^2)[a]	29.82 ± 0.07	20.99 ± 0.08
B (GeV^{-2})	9.60 ± 0.25	7.8 ± 0.3
C (GeV^{-4})	2.25 ± 0.50	0.8 ± 0.4
χ^2/NDF	12/16	9/16

[a] Optical Theorem value neglecting the real part of the elastic amplitude.

Table 2. Total and elastic cross sections and their ratios for π^+p and K^+p interactions at 250 GeV/c

	π^+p	K^+p
σ_{tot} (mb)[1]	24.16 ± 0.03	20.27 ± 0.04
σ_{el} (mb)	3.30 ± 0.11	2.76 ± 0.10
σ_{el}/σ_{tot} (mb)	0.136 ± 0.004	0.136 ± 0.005

FIGURE CAPTIONS

Fig.1 Differential cross sections $d\sigma/dt$ (a) for π^+p and (b)for K^+p collisions at 250 GeV/c. Solid lines are results of fits to the expression $A\exp(Bt+Ct^2)$. The values of A, B and C are given in Table 1

Fig.2 Slope of the differential cross section $d\sigma/dt$ (a) for π^+p and (b) for K^+p collisions at $t=-0.2$ GeV^2, as a function of s, the centre of mass energy squared. Curves are fits to $a+b\ln s/s_0$, ($s_0=1$ GeV^2), with a and b as given in the text

Fig.3 Total elastic cross sections (a) for π^+p and (b) for K^+p collisions, as a function of s, the centre of mass energy squared

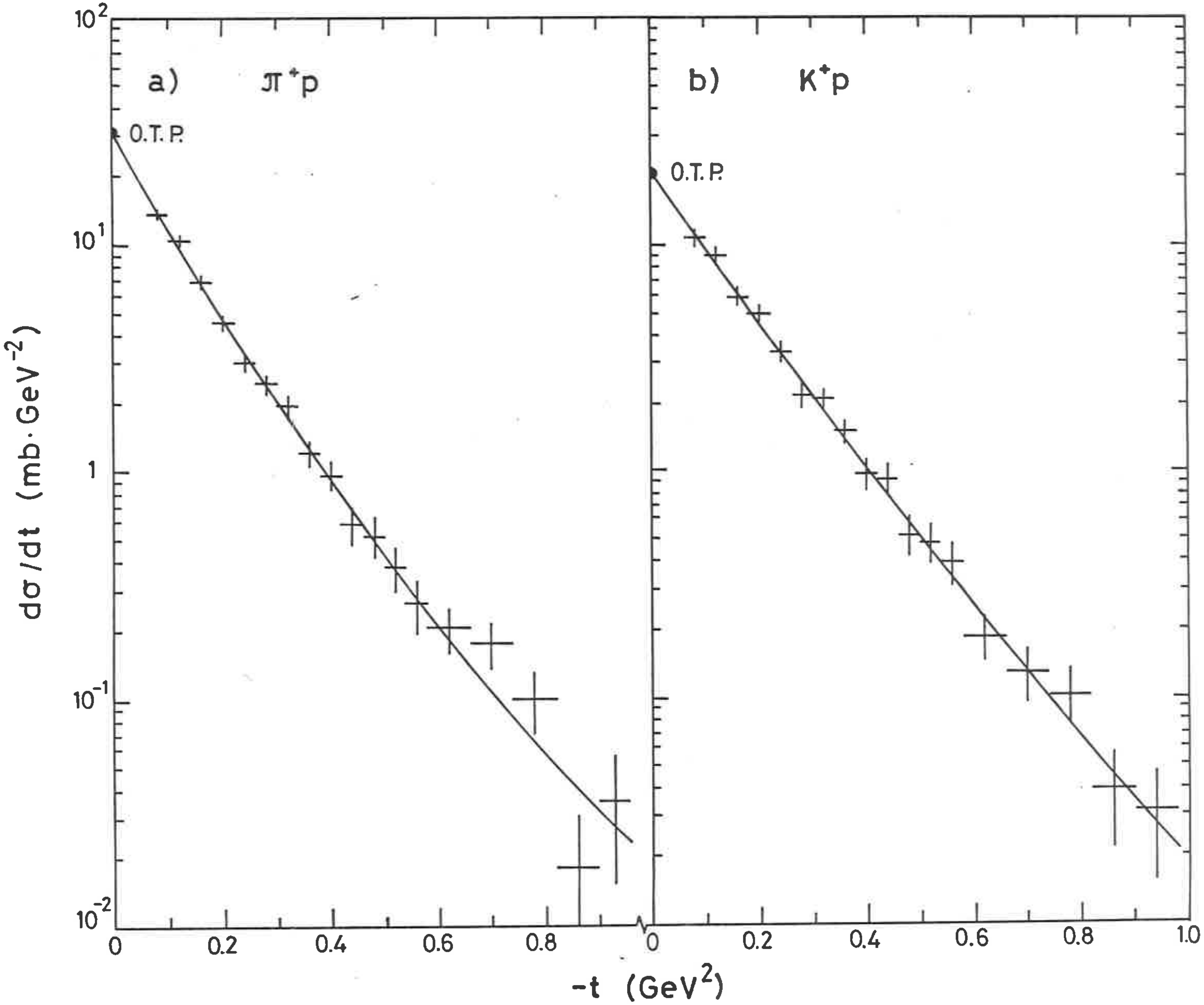
a) π⁺p
b) K⁺p
O.T.P.
O.T.P.
dσ/dt (mb·GeV⁻²)
10²
10¹
1
10⁻¹
10⁻²
0
0.2
0.4
0.6
0.8
1.0
-t (GeV²)

Fig.1

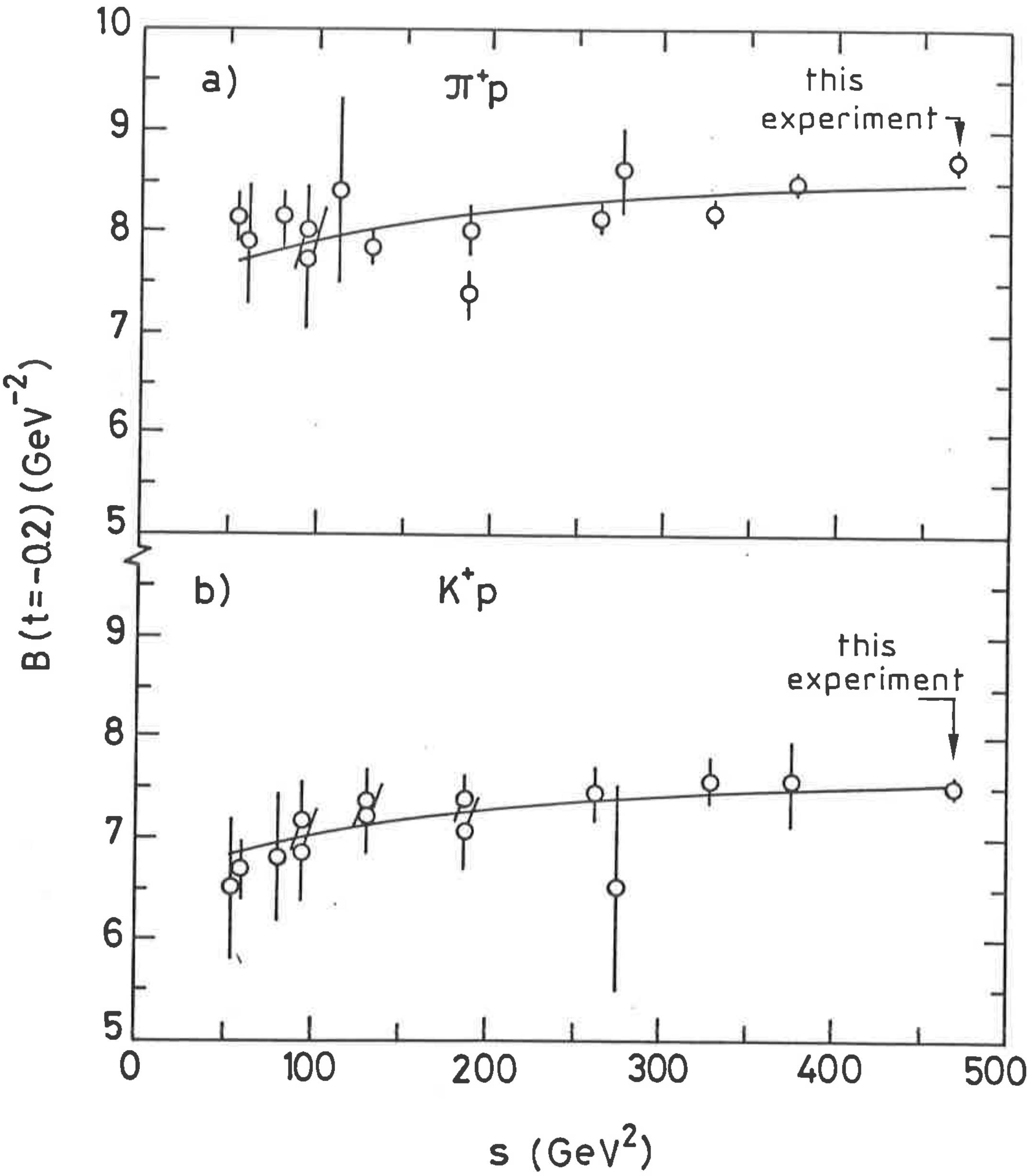

Fig. 2

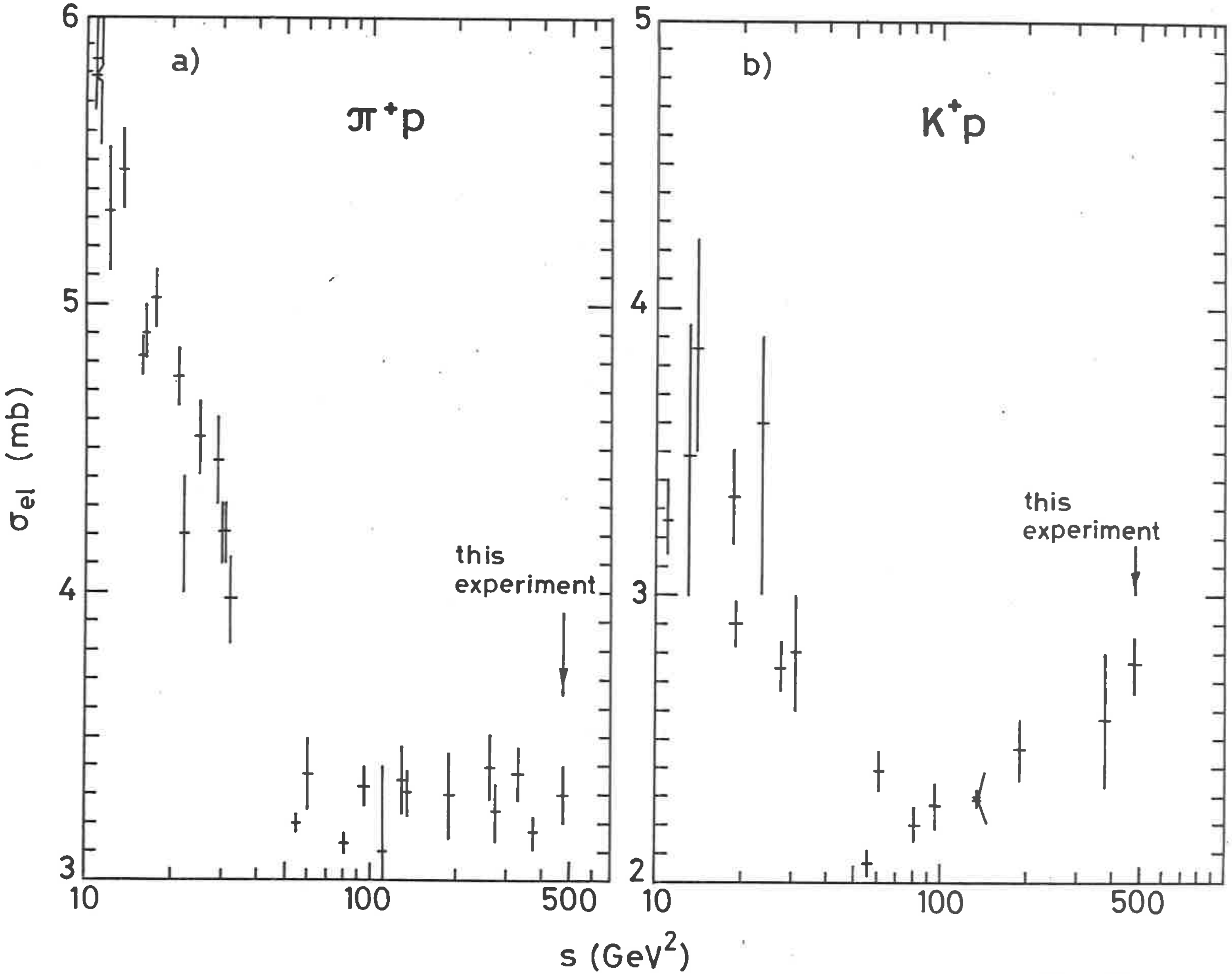

a)
π^+p
b)
K^+p
this experiment
this experiment
σ_{el} (mb)
s (GeV^2)
6
5
4
3
5
4
3
2
10
100
500
10
100
500

Fig. 3